

# Mechanism of the laser initiated ultrafast intracuster reaction in $\text{Ba}\cdots\text{FCH}_3$ and $\text{Ba}\cdots\text{FCD}_3$

V. Stert, H.-H. Ritze, P. Farmanara and W. Radloff\*

Max-Born-Institut für Nichtlineare Optik und Kurzzeitspektroskopie, Max-Born-Str. 2A, D-12489 Berlin, Germany

Received 22nd May 2001, Accepted 6th July 2001

First published as an Advance Article on the web 23rd August 2001

The dynamics of the intracuster reaction  $\text{Ba}\cdots\text{FCH}_3 \rightarrow \text{BaF} + \text{CH}_3$  in the van der Waals complex of barium and monofluoromethane ( $\text{CH}_3\text{F}$  or  $\text{CD}_3\text{F}$ ) initiated by resonant excitation to its electronic  $\tilde{A}$  state has been analyzed on the femtosecond timescale. To elucidate the mechanism we have compared the results of pump-probe experiments for the two complexes  $\text{Ba}\cdots\text{FCH}_3$  and  $\text{Ba}\cdots\text{FCD}_3$ , both excited by 120 fs laser pulses at the resonant wavelength of 618 nm. The measured decay times of the parent ion signals are  $\tau_{\text{IC}} = 270 \pm 30$  fs for  $\text{Ba}\cdots\text{FCH}_3$  and  $\tau_{\text{IC}} = 430 \pm 20$  fs for  $\text{Ba}\cdots\text{FCD}_3$ . The detailed analysis is based on the *ab initio* calculated potential energy surfaces of the parent complex. It is found that the reaction proceeds *via* the next lower electronic  $\tilde{A}'$  state of the complex which is populated after the initial  $\tilde{A}$  state excitation by internal conversion with the time constant  $\tau_{\text{IC}}$ . The subsequent BaF formation out of the intermediate  $\tilde{A}'$  state is restricted to very short times of about 50 fs for both parent clusters due to the competing dissociation of the complex ( $\text{Ba}\cdots\text{FCH}_3 \rightarrow \text{Ba} + \text{CH}_3\text{F}$ ). Thus, the effective formation times for the BaF reaction products exceed only slightly the obtained time constants  $\tau_{\text{IC}}$  for internal conversion.

## 1 Introduction

The harpooning reaction was originally studied in crossed molecular beams of alkali-metal atoms and halide molecules (see *e.g.* ref. 1 and 2). The fast reaction mediated by an electron transfer is suggested to proceed *via* an intermediate state with a reaction time in the sub-picosecond region. Direct observation of the ultrafast process in crossed molecular beams is impossible. To follow the ultrafast reaction in real-time the reactants have to be prepared in a weakly bound van der Waals complex in order to guarantee a well defined starting time. Such experiments with fs time resolution have been carried out until recently only for molecule-molecule complexes<sup>3</sup> whereas the earlier experiments with alkali-metal atom<sup>4</sup> and alkaline-earth-metal atom<sup>5</sup> plus halide complexes were conducted with ns laser pulses.

Recently we have reported the femtosecond time-resolved observation of an intracuster harpooning reaction in the  $\text{Ba}\cdots\text{FCH}_3$  complex. In the experiments we used the spectroscopic data of this complex obtained by Gonzalez-Ureña's group<sup>6,7</sup> by depletion spectroscopy with ns laser pulses: two resonances at wavelengths 618.2 nm (2.0 eV) and 550 nm (2.25 eV) have been defined as the  $\tilde{A}$  and  $\tilde{B}$  electronic states of the  $\text{Ba}\cdots\text{FCH}_3$  complex. The ionization potential (IP) was found to be 4.5 eV. On the basis of these results we have excited the complex resonantly with 120 fs laser pulses at 618 nm to start the intracuster reaction. After ionization with time-delayed probe pulses at 267 nm (4.65 eV)<sup>8</sup> or at 400 nm (3.1 eV)<sup>9</sup> the decay of the parent ion signal and the formation of the BaF product ion signal were detected. In both cases we found a lifetime of  $(270 \pm 30)$  fs for the parent cluster  $\text{Ba}\cdots\text{FCH}_3$  in the initially excited electronic state. Because the stable BaF product was formed with nearly the same time constant we have tentatively defined this time as the overall reaction time. Analysis of the product channel reveals a second contribution to the  $\text{BaF}^+$  signal which shows roughly the same time depen-

dence as the parent signal and, hence, was assigned as a fragment of the parent ion.

To elucidate the energetics of the intracuster reaction in  $\text{Ba}\cdots\text{FCH}_3$  we have first confirmed, by measurements of the fluence dependences, that the parent ion signal is obtained by only one pump photon ( $h\nu_1 = 2$  eV) and one probe photon ( $h\nu_2 = 3.1$  eV) and the stable BaF product is also ionized by only one probe photon. Thus, by determination of the kinetic energies of the two products BaF and  $\text{CH}_3$  (see ref. 9) and the kinetic energy of the photoelectron ejected after the ionization of the BaF product<sup>10</sup> we obtained the complete energetic characterization of the reaction. The results are summarized in Fig. 1. The excited electronic states of the parent complex displayed in Fig. 1 are correlated to the known electronic levels of the Ba atom. As can be seen, the BaF product is preferentially formed in its vibrationally excited electronic B state.

The main topic of the present paper is the elucidation of the intermediate steps leading from the initially excited state of the parent complex at the starting time of the reaction to the stable final product BaF. Here, the crucial point is the negative electron affinity of  $\text{FCH}_3$  in its equilibrium geometry<sup>11</sup> which causes an energetic barrier (see Fig. 1) with regard to the electron transfer from the excited Ba atom to the F atom as the basis for the harpooning reaction. Indeed, no reaction has been observed in experiments with crossed molecular beams of Ba and  $\text{CH}_3\text{F}$  ( $v = 0$ ).<sup>12</sup> Only the stretch of the C–F bond by vibrational excitation can lead to a positive electron affinity and, thus, charge transfer. On the other hand, according to the spectroscopic measurements<sup>6</sup> and our theoretical studies (see below) the resonant excitation at 618 nm is identified as the transition from the vibronic ground state  $\tilde{X}$  ( $v'' = 0$ ) to the lowest vibrational level ( $v' = 0$ ) of the excited electronic  $\tilde{A}$  state of  $\text{Ba}\cdots\text{FCH}_3$ . Hence, the necessary vibrational energy for the C–F stretch is not available and can only be gained by internal conversion from the  $\tilde{A}$  state to the lower-lying excited electronic states. For  $C_{3v}$  symmetry of the parent

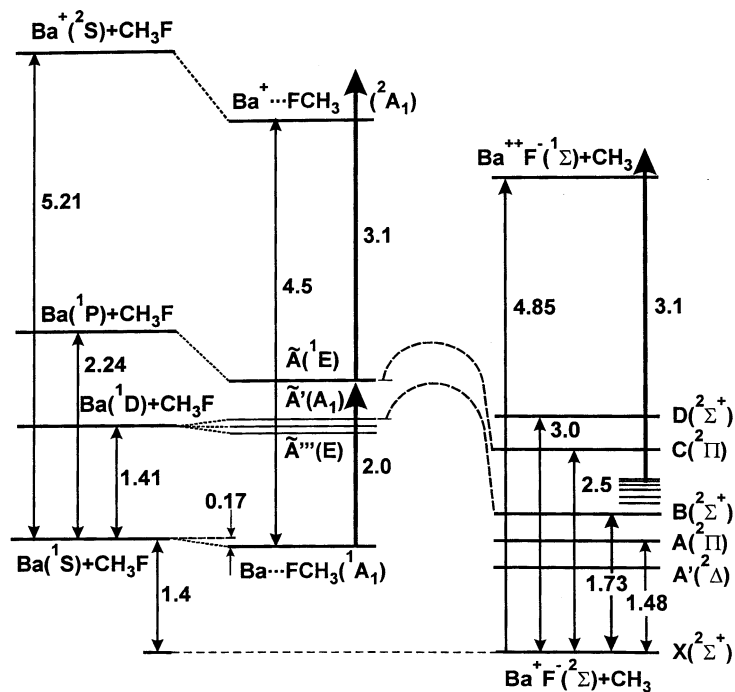


Fig. 1 Energy diagram of  $\text{Ba}\cdot\cdot\text{FCH}_3$  and related species (cf. ref. 9). All energies are given in eV.

complex, which is realized in a good approximation (see below), three electronic states  $\tilde{A}'$ ,  $\tilde{A}''$ ,  $\tilde{A}'''$  corresponding to the  $^1\text{D}$  state of Ba are localized below the  $\tilde{A}$  state (cf. Fig. 1). The potential energies of these states have not been determined previously either experimentally or theoretically.

In the following we describe the results of our studies which strongly suggest the internal conversion from the  $\tilde{A}$  to the  $\tilde{A}'$  state and consecutive processes as the relevant intermediate steps of the intracuster reaction in  $\text{Ba}\cdot\cdot\text{FCH}_3$ . In the next section we discuss the results of *ab initio* calculations of the corresponding potential curves for the ground and excited electronic states of interest. In order to probe the necessity of vibrational excitation of the  $\text{FCH}_3$  part in the complex during the reaction we have studied the dynamics of the reaction in the deuterated complex  $\text{Ba}\cdot\cdot\text{FCD}_3$ . The corresponding experiment and the results are described in sections 3 and 4. The significantly increased reaction time, up to 430 fs, clearly demonstrates the inclusion of the molecular vibrations in the reaction dynamics and, thus, leads to our present understanding of the pathways of the intracuster reaction in  $\text{Ba}\cdot\cdot\text{FCH}_3$ , as discussed in section 5. Further evidence is deduced from the results of time-resolved photoelectron spectroscopy<sup>10</sup> which confirm the conclusions drawn from the present studies.

## 2 *Ab initio* calculations

For an understanding of the intracuster reaction mechanism theoretical studies of the excited electronic states are necessary. As, up to now, no *ab initio* calculations regarding  $\text{Ba}\cdot\cdot\text{FCH}_3$  are available we will compute in the following the potential energy surfaces to clarify the geometry and energetics of this complex. The frequencies and the wavefunctions of the intermolecular stretching vibrations of  $\text{Ba}\cdot\cdot\text{FCH}_3$  in different electronic states will be determined, allowing the calculation of the relevant Franck–Condon factors. This will enable us to find out which vibronic levels are optically excited in the experiment. In the next step an estimation of the nonadiabatic interaction between the neighbouring  $\tilde{A}$  and  $\tilde{A}'$  states and potential calculations along the reaction coordinate will be given, to analyze the pathway and the time range of the  $\text{BaF} + \text{CH}_3$  production. As will be shown, this reaction

competes with fragmentation into  $\text{Ba} + \text{CH}_3\text{F}$ . Using the calculated potential energy curves of the  $\tilde{X}$  and  $\tilde{A}'$  electronic states we will simulate the pump–probe signal *via* the hitherto spectroscopically unknown  $\tilde{A}'$  state as a function of the pump photon energy. This allows us to test the quality of the theoretical results by comparison with the related experimental results.

### 2.1 Computational details

For the *ab initio* calculations of the  $\text{Ba}\cdot\cdot\text{FCH}_3$  potential energy surfaces we used the MOLPRO program package.<sup>13</sup> The contribution of the inner 46 electrons of the barium atom was described by the effective core potential MBS-ECP2.<sup>14</sup> The remaining 10 electrons were considered by taking the basis set (6s7p6d3f)/[3s3p6d3f]. Here we used the s and p functions given in ref. 14 augmented by s(0.008) and p(0.008). Then we added d functions with exponents 0.966 32, 0.893 83, 0.273 20, 0.103 89, 0.035 58 and 0.010. The exponents of the f functions were 0.70, 0.35 and 0.12. For fluorine the s, p and d basis functions of the aug-cc-pVTZ basis set were taken. To describe the F electron affinity properly some diffuse functions were added:<sup>11</sup> s(0.03, 0.0078, 0.003, 0.001), p(0.070, 0.020) and d(0.14). Thus, it results in a (15s8p4d)/[9s6p4d] basis set. For carbon we also used the s, p and d basis functions of the aug-cc-pVTZ basis set augmented by s(0.010, 0.0025), p(0.0086) and d(0.057)<sup>11</sup> leading to the (13s7p4d)/[7s5p4d] basis set. The hydrogen atom was described by the s and p functions of aug-cc-pVTZ yielding a (6s3p)/[4s2p] basis set.

The basis sets used were tested in complete active space self consistent field (CASSCF) calculations followed by the multi-reference configuration interaction (MRCI) procedure of the 3 lowest Ba, the 5 lowest BaF electronic states and the  $\text{Ba}^+$  and  $\text{BaF}^+$  ground states. The calculated excitation energies and ionization potentials differed by less than 0.1 eV from the known experimental values.

The state-averaged CASSCF method was applied to the  $\text{Ba}\cdot\cdot\text{FCH}_3$  complex, assuming at least  $C_s$  symmetry. The two Ba valence electrons were distributed among 10 active orbitals. For the subsequent MRCI + Q (with Davidson correction) procedure only the carbon and fluorine 1s electrons were frozen.

## 2.2 Theoretical results

In Fig. 2 the results of the calculated Ba $\cdot\cdot$ FCH<sub>3</sub> interaction energies for the ground and the lowest excited electronic states and the ground cationic state are given as a function of the Ba–C distance. The geometry of the fluoromethane molecule was optimized by minimizing the energy for a given Ba–C distance. In these calculations we assumed the stronger restriction to C<sub>3v</sub> symmetry of Ba $\cdot\cdot$ FCH<sub>3</sub> which is justified because the deviations from C<sub>s</sub> symmetry are negligibly small (see below). Using the calculated binding energies (*D<sub>e</sub>*) for Ba $\cdot\cdot$ FCH<sub>3</sub> in the different electronic states (*cf.* Table 1), the known electronic excitation energies and the ionization potential of the Ba atom we found the ionization potential IP<sub>th</sub> = 4.55 eV of the complex and the  $\tilde{X} \rightarrow \tilde{A}$  (0–0) transition frequency  $\tilde{\nu}_{th} = 16\,150\text{ cm}^{-1}$ . These values agree very well with the quantities IP<sub>exp</sub> = (4.5 ± 0.1) eV and  $\tilde{\nu}_{exp} = 16\,174\text{ cm}^{-1}$  (2.0 eV) determined experimentally.<sup>6</sup>

In Table 1 the equilibrium geometries obtained for the electronic states of interest assuming C<sub>3v</sub> symmetry are given. (There also the CH<sub>3</sub>F equilibrium geometries calculated in the present work (a) and the experimentally revealed values (b) are compared.)

To test the validity of the assumed C<sub>3v</sub> symmetry we have also varied the angle Ba–F–C, conserving C<sub>s</sub> symmetry. Whereas the cationic equilibrium geometry indeed shows C<sub>3v</sub> symmetry the situation is different for the neutral  $\tilde{X}$  and  $\tilde{A}$  states. The true equilibrium geometry of the  $\tilde{X}$  state is bent with a Ba–F–C angle of about 163°. However, the minimum of the C<sub>3v</sub> symmetric complex is only about 4 cm<sup>-1</sup> higher. After quantization of the Ba–F–C bending motion we have found that the maximum of the ground state wavefunction is achieved for the Ba–F–C angle of 180°, *i.e.*, in the ground vibronic state the Ba $\cdot\cdot$ FCH<sub>3</sub> complex can be assumed to be a quasi-symmetric top. The vibrational frequency of the intermolecular Ba–FCH<sub>3</sub> stretching vibration was calculated to be  $\tilde{\nu}_{stretch} = 120\text{ cm}^{-1}$ .

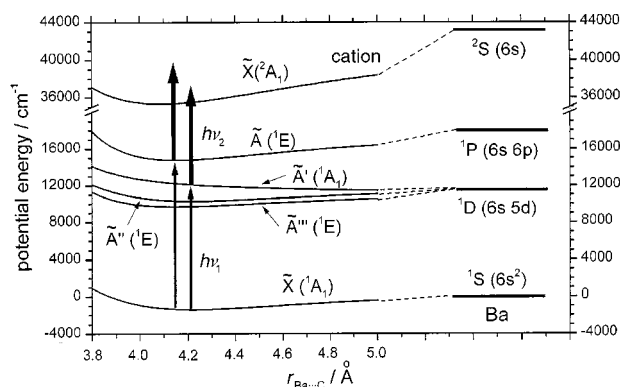


**Fig. 2** Potential energies of the Ba $\cdot\cdot$ FCH<sub>3</sub> complex as a function of the Ba $\cdot\cdot$ C distance for the electronic ground state ( $\tilde{X}$ ), the excited states ( $\tilde{A}$ ,  $\tilde{A}'$ ,  $\tilde{A}''$ ,  $\tilde{A}'''$ ) and the ionic ground state. The correlation to the Ba atom states is shown. Pump photon energy:  $h\nu_1$ , probe photon energy:  $h\nu_2$ .

**Table 1** Equilibrium geometries and binding energies *D<sub>e</sub>* of Ba $\cdot\cdot$ FCH<sub>3</sub> in the ground ( $\tilde{X}$ ) and excited electronic ( $\tilde{A}$ ) state and in the ionic ground state. The Ba–F–C angle is assumed to be 180° (see text). The calculated equilibrium geometry of CH<sub>3</sub>F<sup>(a)</sup> is compared with that of CH<sub>3</sub>F<sup>(b)</sup> obtained experimentally<sup>21</sup>

Species, State	$r_{\text{Ba-F}}/\text{Å}$	$r_{\text{C-F}}/\text{Å}$	$r_{\text{C-H}}/\text{Å}$	$\angle_{\text{H-C-F}}/^\circ$	$D_e/\text{cm}^{-1}$
CH <sub>3</sub> F <sup>(a)</sup> , $\tilde{X}$	—	1.395	1.099	108.5	—
CH <sub>3</sub> F <sup>(b)</sup> , $\tilde{X}$	—	1.382	1.095	108.5	—
Ba $\cdot\cdot$ FCH <sub>3</sub> , $\tilde{X}$	2.817	1.422	1.090	108.2	1350
[Ba $\cdot\cdot$ FCH <sub>3</sub> ] <sup>*</sup> , $\tilde{A}$	2.743	1.450	1.085	107.6	3260
[Ba $\cdot\cdot$ FCH <sub>3</sub> ] <sup>+</sup> , $\tilde{X}$	2.610	1.480	1.083	106.9	6710

The  $\tilde{A}$  electronic state (due to the notation<sup>6</sup>) is twofold degenerate in C<sub>3v</sub> symmetry. In general, for lower symmetry this degeneracy is removed by the Jahn–Teller effect. We have varied the Ba–F–C angle and found that the linear Jahn–Teller effect is negligibly small. But the quadratic Jahn–Teller effect (Renner–Teller-like interaction) has to be taken into account. The global potential minimum of the  $\tilde{A}$  state is achieved for a bent configuration where the Ba–F–C angle is 152°. This minimum is about 25 cm<sup>-1</sup> deeper than the minimum for the C<sub>3v</sub> symmetric configuration. We have calculated the lower vibrational levels and the corresponding wavefunctions for the intermolecular degrees of freedom (Ba–FCH<sub>3</sub> stretching and bending) under consideration of the Jahn–Teller effect. (The corresponding details are beyond the scope of the present paper and will be presented in a forthcoming publication.) The probability distribution of the lowest vibrational level in the  $\tilde{A}$  electronic state exhibits a maximum for the Ba–F–C angle of 180°. Thus, it is reasonable to describe the complex in this state as a quasi-symmetric top. The intermolecular stretching frequency was found to be  $\tilde{\nu}_{stretch} = 145\text{ cm}^{-1}$ . This value is nearly the same as the experimentally observed value (154 cm<sup>-1</sup>).<sup>7</sup> Our calculated Franck–Condon factor for the  $\tilde{X} \rightarrow \tilde{A}$  (0–0) transition was larger than 0.8, *i.e.*, predominantly the ground vibrational level of the  $\tilde{A}$  electronic state is optically excited, even if spectrally broad femtosecond laser pulses are used.

Now the question arises: How can the depopulation of the primarily excited level (by the pump pulse), which according to our previous experiments<sup>8,9</sup> proceeds on the sub-ps time-scale, be understood? Supposing an internal conversion as a possible way we looked first for conical intersections of the  $\tilde{A}$  state potential energy surface with those of other states near the equilibrium geometry but did not find any. The next state below the  $\tilde{A}$  electronic state (denoted by  $\tilde{A}'$ ) is not degenerate. Here, the density of the Ba 5d electron is oriented along the symmetry axis of the complex. Thus, only a weak bonding state arises (*D<sub>e</sub>* = 125 cm<sup>-1</sup>) with an equilibrium distance  $r_{\text{Ba-C}} = 6.2\text{ Å}$ . This state is repulsive for  $\tilde{X}$  and  $\tilde{A}$  equilibrium geometries. The vertical  $\tilde{A} \rightarrow \tilde{A}'$  energy gap for the  $\tilde{A}$  equilibrium geometry is about 2650 cm<sup>-1</sup> (see Fig. 3). This value is of the order of the C–H degenerate stretching frequencies, thus allowing a nonadiabatic  $\tilde{A} \leftrightarrow \tilde{A}'$  coupling with the degenerate C–H stretching mode as the promoting mode. In preliminary calculations we estimated the lifetime of the ground vibrational level of the  $\tilde{A}$  state in Ba $\cdot\cdot$ FCH<sub>3</sub> to lie in the sub-picosecond region. Here, we used the frequency of the degenerate C–H stretch mode  $\nu_4(\text{E}) = 2999\text{ cm}^{-1}$  of CH<sub>3</sub>F<sup>15</sup> as the promoting mode. This mode was selected for symmetry reasons because the vibronic symmetry is conserved for non-adiabatic coupling. As the optically excited electronic state  $\tilde{A}$  is degenerate (E) and the  $\tilde{A}'$  state is totally symmetric (A<sub>1</sub>), the ground vibrational level of the  $\tilde{A}$  electronic state can only couple with a degenerate vibrational level of the  $\tilde{A}'$  state. In principle, other degenerate vibrations of the complex can also act as promoting modes, however, their frequencies are considerably lower. Thus, further vibrations would have to be included as acceptor modes in this case. This would only lead to relatively small nonadiabatic coupling constants because

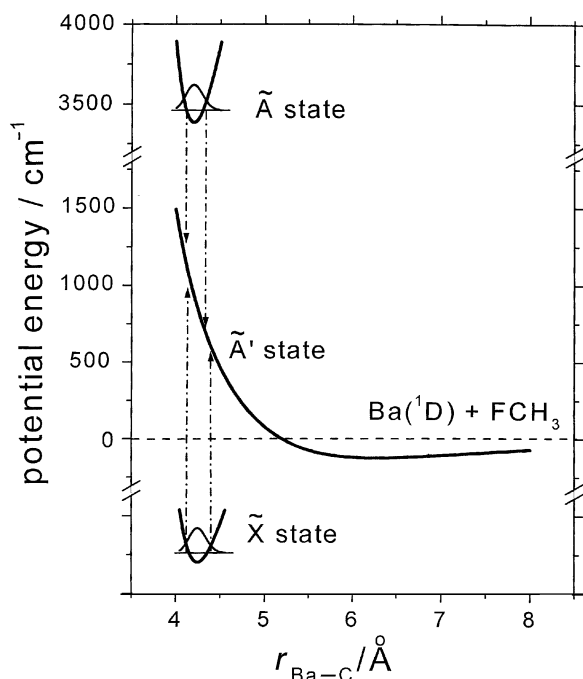


**Fig. 3** Potential energy of the  $\tilde{A}'$  state as a function of the Ba $\cdots$ C distance (cf. Fig. 2). The dashed vertical lines represent the limits of the Franck–Condon regions for the  $\tilde{X}(v=0) \rightarrow \tilde{A}'(v \neq 0)$  transition and the  $\tilde{A}'(v=0) \rightarrow \tilde{A}'(v \neq 0)$  internal conversion.

the geometry of the  $\text{CH}_3\text{F}$  constituent is nearly equal in the  $\tilde{A}$  and  $\tilde{A}'$  state and, hence, the corresponding Franck–Condon factors for these acceptor modes should be poor for  $\Delta v \neq 0$ .

The estimation of the lifetime due to nonadiabatic  $\tilde{A} \leftrightarrow \tilde{A}'$  coupling can be briefly described as follows: first the electronic part of the  $\tilde{A} \leftrightarrow \tilde{A}'$  coupling matrix element is found analytically using the MOLPRO package. Then the vibrational matrix element for the  $v=0 \rightarrow v=1$  transition of the  $\nu_4$  mode is calculated in the harmonic oscillator approximation. Finally, according to Fermi's Golden Rule, we obtained a transition rate per unit time to the unbound level of the  $\tilde{A}'$  state lying  $2999 \text{ cm}^{-1}$  below the first optically excited level. Here the one-dimensional ( $r_{\text{Ba-C}}$ ) Franck–Condon-type overlap between the initial vibrational wavefunction of the  $\tilde{A}$  state and the unbound  $\tilde{A}'$  state wavefunction is calculated. Since the corresponding frequency ( $\nu_4$ ) for  $\text{CD}_3\text{F}$  is significantly lower ( $2259 \text{ cm}^{-1}$ ), the  $\tilde{A} \leftrightarrow \tilde{A}'$  Franck–Condon-type overlap is smaller for  $\text{Ba}\cdots\text{FCD}_3$  than for  $\text{Ba}\cdots\text{FCH}_3$  due to the larger difference between the  $\nu_4$  value and the vertical  $\tilde{A} \leftrightarrow \tilde{A}'$  energy gap. Thus, a larger lifetime is expected for the deuterated than for the undeuterated complex.

To test the possibility of BaF production starting with  $\text{Ba}\cdots\text{FCH}_3$  in its vibrationally excited  $\tilde{A}'$  state we have calculated the corresponding adiabatic potential curve as a function of the C–F distance for fixed  $r_{\text{Ba-C}} = 4.2 \text{ \AA}$  assuming  $C_{3v}$  symmetry and optimizing the  $\text{CH}_3$  geometry for each value  $r_{\text{C-F}}$  (see Fig. 4). Starting with  $r_{\text{C-F}} = 1.40 \text{ \AA}$ , for increasing distance  $r_{\text{C-F}}$  the potential energy increases up to the top of the barrier at  $r_{\text{C-F}} = 1.63 \text{ \AA}$  where the charge transfer to  $\text{Ba}^+\text{F}^-\cdots\text{CH}_3$  begins. At this point the  $\text{CH}_3$  geometry is characterized by  $\angle \text{F-C-H} = 95^\circ$  and  $r_{\text{C-F}} = 1.08 \text{ \AA}$  which is similar to the transition state in the ion  $[\text{Ca}\cdots\text{F}\cdots\text{CH}_3]^+$ .<sup>17</sup> For larger  $r_{\text{C-F}}$  values this adiabatic potential correlates to  $\text{BaF}(\text{B}^2\Sigma^+) + \text{CH}_3$ . The top of the barrier is slightly lower than the energy of the ground vibrational level of the  $\tilde{A}$  electronic state, i.e., after internal  $\tilde{A} \rightarrow \tilde{A}'$  conversion the BaF formation is energetically possible. However, in our model, after internal conversion the C–H stretching vibration is initially excited in the  $\tilde{A}'$  state, thus, a strong Fermi-like coupling to the C–F vibration is required to overcome very quickly the

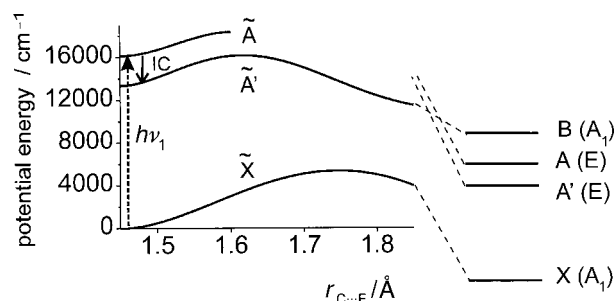


**Fig. 4** Calculated potential energies of the  $\tilde{X}$  and  $\tilde{A}'$  states as a function of the C $\cdots$ F distance for  $C_{3v}$  symmetry. The Ba $\cdots$ C distance is fixed ( $r_{\text{Ba-C}} = 4.2 \text{ \AA}$ ) and the other degrees of freedom are relaxed. The correlation to the energetic structure of BaF is shown on the right-hand side (BaF and  $\text{CH}_3$  are well separated).

barrier to the BaF formation. The charge transfer reaction has to be fast because the Ba–C distance rapidly increases due to the repulsive part of the  $\tilde{A}'$  potential. We have found that for  $r_{\text{Ba-C}} > 4.4 \text{ \AA}$  the barrier becomes higher than the energy of the  $\tilde{A}'(v=0)$  state.

Furthermore, we have calculated the wavelength dependence of the absorption from the ground vibronic state to the repulsive part of the  $\tilde{A}'$  state, considering only the intermolecular stretch degree of freedom. Taking into account the spectral width of the laser pulses (about 7 nm) we obtained the theoretical curve (full line in Fig. 5) for the pump–probe signals of this transition. The maximum of the absorption is achieved at a wavelength of 745 nm ( $13\,500 \text{ cm}^{-1}$ ).

### 3 Experimental

As described in detail in our earlier papers<sup>8,9</sup> the weakly bound  $\text{Ba}\cdots\text{FCH}_3$  or  $\text{Ba}\cdots\text{FCD}_3$  complexes were prepared in a molecular beam by the adiabatic expansion of a gas mixture containing laser desorbed Ba vapor and molecular  $\text{CH}_3\text{F}$  or  $\text{CD}_3\text{F}$  gas (10%) in He (1 bar) carrier gas. The interaction channel of the vaporization source was cooled to about  $-130^\circ\text{C}$  in order to enlarge the cluster concentration. The energy of the focused radiation (diameter: 0.2–0.3 mm) of the vaporization laser (SHG of a Nd:YAG laser) was restricted to low values (0.7 mJ) in order to reduce chemical reactions in the gas mixture near the laser-heated Ba rod. The molecular beam was crossed by two weakly focused copropagating laser beams in the interaction region of a time-of-flight (TOF) mass spectrometer. The laser system used was a commercial Ti:sapphire laser and amplifier system (Clark MXR) tuned to 800 nm (1.55 eV) which is combined with a commercial OPA system (Clark I-GOR-SHG). The second harmonic of the OPA signal was used for the excitation of the clusters. At first its wavelength was tuned across the region 725–760 nm in

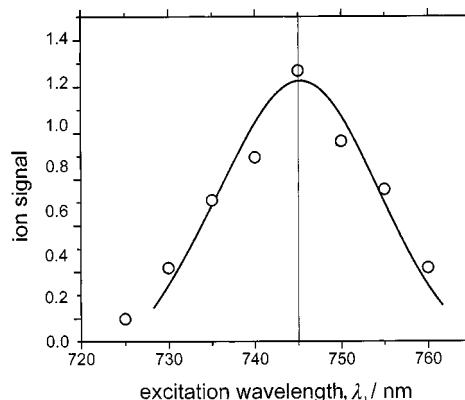


**Fig. 5** Measured  $\text{Ba}\cdots\text{FCH}_3^+$  ion signals obtained by excitation of the  $\tilde{A}'$  state with pump pulses at different wavelengths  $\lambda_1$ . The probe wavelength is fixed at  $\lambda_2 = 400 \text{ nm}$ . The solid line represents the corresponding theoretical curve explained in the text.

which the resonance to the  $\tilde{A}'$  state of  $\text{Ba}\cdots\text{FCH}_3$  was expected according to the theoretical estimations in section 2. In the second part of the experiments it was tuned to the known resonance of the  $\tilde{X} \rightarrow \tilde{A}$  transition in the  $\text{Ba}\cdots\text{FCH}_3$  complex at 618 nm (2 eV). The second harmonic of the Ti : Sapphire laser at 400 nm (3.1 eV) was applied to probe the excited clusters and the products by ionization. The width (FWHM) of the laser pulses was about 120 fs. Typical values of the laser fluences were about  $0.2 \text{ mJ cm}^{-2}$  for the pump pulse at 618 nm and about  $1.5 \text{ mJ cm}^{-2}$  for the probe pulse at 400 nm.

The ion signals were detected by a microchannel plate detector in the TOF mass spectrometer, digitized by a fast digital oscilloscope (Tektronix TDS 520A) and stored and processed by a PC.

A standard delay line was used to scan the delay time between the pump and the probe pulses. At a repetition frequency of 33 Hz the mass spectra were accumulated typically for 50 laser pulses at each delay time  $\tau$  and averaged over 50 up and down scans of the delay line.

#### 4 Experimental results

Prior to the description of the experiments on the reaction dynamics in  $\text{Ba}\cdots\text{FCD}_3$  initiated by excitation of the  $\tilde{A}$  state at 618 nm (2.0 eV) we first report the experimental verification of the  $\tilde{A}'$  state's potential energy as predicted theoretically by *ab initio* calculations (cf. section 3). We measured the pump-probe signals of the  $\text{Ba}\cdots\text{FCH}_3^+$  ions as a function of the pump wavelength  $\lambda_1$  tuned through the region 725–760 nm (1.71–1.63 eV). The probe pulse fixed at the wavelength of 400 nm (3.1 eV) was delayed only slightly with respect to the pump pulse such that the pump-probe ion signal was always maximum. The measured signals represented in Fig. 5 agree excellently with the theoretical curve (solid line). The signal maximum found experimentally at  $\lambda_1 = 745 \text{ nm}$  (1.67 eV) confirms the calculated  $\tilde{X} \rightarrow \tilde{A}'$  transition frequency of  $13\,500 \text{ cm}^{-1}$  (1.67 eV). The measured spectral width of the two-photon absorption process completely agrees with the Franck–Condon width of the corresponding transitions determined theoretically.

The time-dependent ion signals for the reaction in  $\text{Ba}\cdots\text{FCH}_3$  initiated by 120 fs laser pulses at 618 nm have already been presented in a previous report.<sup>9</sup> Here we conducted the experiment for the deuterated complex  $\text{Ba}\cdots\text{FCD}_3$  with identical laser parameters, i.e. the  $\text{Ba}\cdots\text{FCD}_3$  complexes are excited by the pump pulse at  $\lambda_1 = 618 \text{ nm}$  and ionized by the probe pulse at  $\lambda_2 = 400 \text{ nm}$ . To confirm the position of the  $\tilde{A}$  state resonance for  $\text{Ba}\cdots\text{FCD}_3$  at 618 nm we tuned the excitation wavelength by  $\pm 4 \text{ nm}$  to 622 and 614 nm, respectively. The measured pump-probe signals (for  $\tau = 0$ ) at both wavelengths are reduced, nearly identically, by a factor of three with respect to the maximum at 618 nm. This corresponds to the expected signal relations for a narrow resonance at 618 nm convoluted with the spectrally broad laser pulses tuned across the resonance. Hence, a possible deviation of the position of the  $\text{Ba}\cdots\text{FCD}_3$  resonance from the known value for  $\text{Ba}\cdots\text{FCH}_3$  is not measurable within the spectral resolution of our laser pulses.

In Fig. 6a the time-dependent ion signal is shown for  $\text{Ba}\cdots\text{FCD}_3$  excited by the pump pulse at  $\lambda_1 = 618 \text{ nm}$  to its  $\tilde{A}$  state and ionized by the probe pulse at  $\lambda_2 = 400 \text{ nm}$ . The formation of the reaction products BaF and Ba is depicted on the same timescale (Fig. 6b and c). The solid lines in Fig. 6 represent the theoretical fit curves according to our model.<sup>18</sup> The resonant coherent interaction of the parent complex with the pump laser field is described by optical Bloch equations with a single-exponential decay of the excited cluster. The time dependence of secondarily populated states is described by rate equations combined with the Bloch equations.

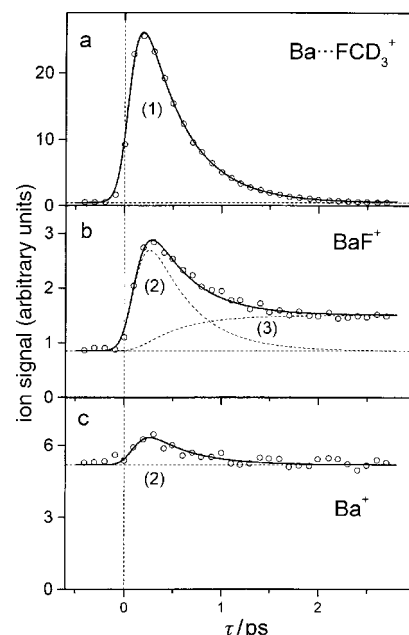


**Fig. 6** Ion signals for  $\text{Ba}\cdots\text{FCD}_3$  (a), BaF (b) and Ba (c) as a function of the delay time  $\tau$  between the pump pulse at 618 nm and probe pulse at 400 nm. The solid lines are theoretical fit curves explained in the text.

Assuming a  $\text{sech}^2(t)$  pulse shape and the pulse width  $\tau_L = 120 \text{ fs}$  we obtained the fit curves by solution of the equations, convolution with the laser pulse shape and optimization with respect to the experimental points. The zero delay time defined consistently by the fitting procedure was confirmed by suitable calibration signals, e.g. the position of the nonresonantly excited parent ion signal (cf. ref. 9). The shift of the maximum of the fit curve with respect to the delay time zero is a sensitive measure for the finite decay time of the excited state and, thus, especially valuable for the determination of lifetimes much smaller than the pulse width.

The time-dependent ion signals in Fig. 6 can be fitted by three different contributions with the notation (1), (2) and (3). The parent ion signal (contribution (1) in Fig. 6a) reflects the exponential decay of the initially excited  $\tilde{A}$  state with a time constant of  $(430 \pm 20) \text{ fs}$ . The accuracy of the obtained decay time is relatively high because of the excellent signal-to-noise ratio of the corresponding measurement. The BaF<sup>+</sup> product signal is superimposed by the contribution (3) of a stable product, formed with nearly the same time constant of 430 fs, and the contribution (2) which resembles the shape of the parent ion signal but is slightly shifted to positive delay times. Careful analysis reveals, for the contribution (2), a formation time of  $(50 \pm 20) \text{ fs}$  and a decay time of 430 fs. Here it has to be remarked that for this intermediate term (2) an identical time-dependent curve is obtained by exchanging the time constants for the formation and decay processes because the rate equations corresponding to the two situations have the same solution.<sup>19</sup> The growth of the stable contribution (3) can be described only roughly by a single-exponential rise time of about 460 fs. As we will see below, the formation of the neutral BaF product proceeds *via* two consecutive processes with time constants of 430 and 50 fs. Thus, the overall formation time of 460 fs exceeds only slightly the time constant of 430 fs. The fits of the terms (2) and (3) are less accurate due to the uncertainties caused by their superposition and due to the fluctuations of the BaF<sup>+</sup> signal (see Fig. 6b).

The weak Ba<sup>+</sup> signal (Fig. 6c) with a time dependence identical to that of the contribution (2) of BaF<sup>+</sup> is caused by absorption of one additional probe photon by the parent ion

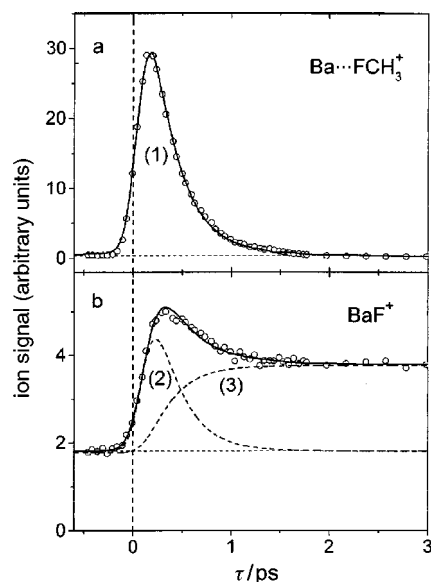


**Fig. 7** Signals of the parent ion  $\text{Ba}\cdots\text{FCH}_3^+$  (a) and product ion  $\text{BaF}^+$  (b) vs. delay time  $\tau$  for  $\lambda_1 = 618$  nm and  $\lambda_2 = 400$  nm (cf. Fig. 6). The solid lines are theoretical fit curves discussed in the text.

(not shown in Fig. 8 below) which may lead to the dissociation of the electronically excited ion state after internal conversion. A further contribution to the  $\text{Ba}^+$  signal resulting from ionization of neutral Ba fragments (see the reaction scheme) is not observed, because the two-probe-photon ionization efficiency is too low. Very recent experiments with a higher probe photon energy of 4.65 eV clearly indicate the formation of neutral Ba fragments in the course of the reaction.<sup>20</sup>

In the light of the detailed fit procedure for  $\text{Ba}\cdots\text{FCD}_3$  we have improved the fit of the time-dependent ion signals for the reaction in  $\text{Ba}\cdots\text{FCH}_3$  measured earlier and already published in ref. 9. As shown in Fig. 7a the parent ion signal  $\text{Ba}\cdots\text{FCH}_3^+$  is characterized by a single-exponential decay with time constant  $(270 \pm 30)$  fs. The fit procedure for the  $\text{BaF}^+$  signal (Fig. 7b) was carried out as above for  $\text{Ba}\cdots\text{FCD}_3$ . Here the contribution (2) is characterized by a formation time of  $(50 \pm 30)$  fs and a decay time of 270 fs. As already mentioned above, the reverse situation with a formation time of 270 fs and a decay time of 50 fs leads to the same ion signal. The contribution (3) is approximated by a single-exponential rise time of about 300 fs which also fits quite well the  $\text{BaF}^+$  formation in two successive steps with time constants of 270 and 50 fs.

## 5 Discussion of the reaction scheme

The fits of the experimental results (Fig. 6 and 7) by the theoretical time-dependent curves were guided by the reaction model which is displayed in Fig. 8. The different contributions (1), (2) and (3) to the signals obtained for the parent and product ions can be understood in a consistent way. According to our theoretical estimations (section 2) contribution (1), which is characterized by an exponential decay of the initially excited  $\tilde{A}$  state, is interpreted as due to internal conversion to the next lower electronic  $\tilde{A}'$  state. The corresponding time constant  $\tau_{\text{IC}}$  is significantly larger for  $\text{Ba}\cdots\text{FCD}_3$  (430 fs) than for  $\text{Ba}\cdots\text{FCH}_3$  (270 fs). As discussed above, the  $\nu_4$  stretch mode of the  $\text{CH}_3\text{F}$  part in the complex as the promoting mode for the nonadiabatic coupling fits quite well the  $\tilde{A} \rightarrow \tilde{A}'$  energy gap in  $\text{Ba}\cdots\text{FCH}_3$ . For  $\text{CD}_3\text{F}$ , however, the energy of the  $\nu_4$  mode is significantly lower and, hence, the larger time constant for the excited  $\tilde{A}$  state is plausible.

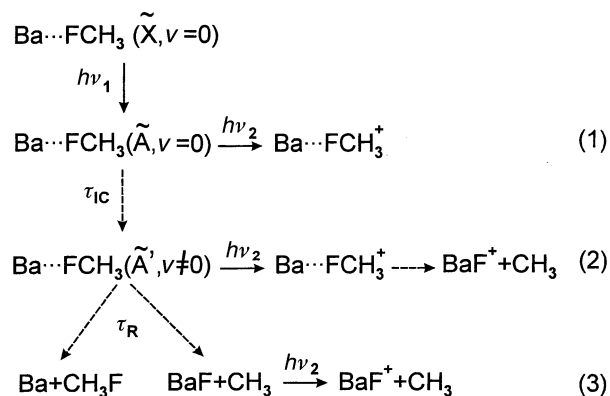


**Fig. 8** Scheme of the intracuster reaction in  $\text{Ba}\cdots\text{FCH}_3$  initiated by excitation to its electronic  $\tilde{A}$  state. The numbers in brackets (1), (2), (3) denote different states of the reaction which contribute to the parent and product ion signals (see text).

A direct proof for the energy transfer due to  $\tilde{A} \rightarrow \tilde{A}'$  internal conversion was obtained by analysis of the corresponding time-resolved photoelectron spectra. In ref. 10 we have confirmed that after absorption of the pump ( $h\nu_1$ ) and probe ( $h\nu_2$ ) photons (at  $\tau = 200$  fs) the parent ion  $\text{Ba}\cdots\text{FCH}_3^+$  (ionization potential IP) contains almost no vibrational energy because the excess energy  $h\nu_1 + h\nu_2 - \text{IP}$  is carried away by the ejected photoelectron. Because the geometries of the parent complex in the excited  $\tilde{A}(^1\text{E})$  state and in the ionic ground state  $\tilde{X}(^2\text{A}_1)$  are quite similar to that of the electronic ground state  $\tilde{X}(^1\text{A}_1)$  (cf. Fig. 2) vibrationless transitions between these states are preferred due to Franck–Condon rules. Thus, dissociation of the parent cluster ions formed *via* the  $\tilde{A}$  state is excluded and no fragments of the contribution (1) occur (see Fig. 8).

In contrast, in the electron spectrum for the  $\text{BaF}^+$  ion we observed a dominant contribution resulting from the parent ion which corresponds to a vibrational energy of about 0.35 eV,<sup>10</sup> *i.e.* exactly that energy expected after the internal conversion from the  $\tilde{A}$  to the  $\tilde{A}'$  state according to the theoretical findings of the present work. At a delay time of  $\tau = 200$  fs after the pump pulse the internal conversion has already led to a population of the  $\tilde{A}'$  state with an increase in its vibrational energy of 0.35 eV. For Franck–Condon reasons the vibrational energy in the ionic ground state agrees with the vibrational energy in the secondarily populated  $\tilde{A}'$  state. On the one hand this vibrational energy in the parent ion will cause its dissociation and the formation of the  $\text{BaF}^+$  fragment (Fig. 8, contribution (2)). On the other hand the correspondingly high vibrational energy in the secondarily populated  $\tilde{A}'$  state is sufficient to overcome the barrier of the reaction in the neutral complex, which consequently proceeds with the time constant  $\tau_{\text{R}} = 50$  fs in competition to the dissociation channel (see Fig. 8, contribution (3)). Hence, the contribution (2) of the  $\text{BaF}^+$  signal should reflect the population of the  $\tilde{A}'$  state by internal conversion with the time constant  $\tau_{\text{IC}}$  (430 fs for  $\text{Ba}\cdots\text{FCD}_3$  and 270 fs for  $\text{Ba}\cdots\text{FCH}_3$ ) and its decay with the time constant  $\tau_{\text{R}} = 50$  fs due to the competing reaction and dissociation processes out of this state. Indeed, the measured  $\text{BaF}^+$  ion signals defined as contribution (2) in Fig. 6b and 7b exhibit exactly these time dependences if we exchange there the time constants for the formation and decay processes. Correspondingly, the contribution (3) of the  $\text{BaF}^+$  signal is formed in two successive steps, *i.e.* first by the population of the intermediate  $\tilde{A}'$  state within  $\tau_{\text{IC}}$  and second by the reaction out of this state within  $\tau_{\text{R}}$ . Because of the relation  $\tau_{\text{R}} \ll \tau_{\text{IC}}$  the resultant formation time of the stable  $\text{BaF}^+$  product is only slightly larger than the time constant  $\tau_{\text{IC}}$  and the formation process can be approximated by a single-exponential curve. This is in full agreement with the fitted curves (3) of the time-

dependent  $\text{BaF}^+$  ion signals for which we have derived an overall BaF formation time of 460 fs for  $\text{Ba}\cdot\cdot\text{FCD}_3$  (see Fig. 6b) and of 300 fs for  $\text{Ba}\cdot\cdot\text{FCH}_3$  (see Fig. 7b).

For the decay of the intermediate state  $\text{Ba}\cdot\cdot\text{FCH}_3(\tilde{A}')$  into two different channels (*cf.* Fig. 8) our analysis reveals only one resultant time constant  $\tau_R$  comprising the decay of the  $\tilde{A}'$  state in the reactive and the non-reactive channel which we cannot separate. Because neither the branching ratios for these two channels nor the ionization probabilities of the intermediate and the final product states are known we have no means to determine explicitly the specific rate constant for the charge transfer process leading to BaF. The formation time for BaF out of the intermediate  $\tilde{A}'$  state is restricted by the resultant decay time  $\tau_R$ .

## 6 Conclusions

In recent studies the intracuster reaction  $\text{Ba}\cdot\cdot\text{FCH}_3 \rightarrow \text{BaF} + \text{CH}_3$  has been found to proceed with an overall time constant of roughly 270 fs.<sup>8,9</sup> Here the resonant excitation to the electronic  $\tilde{A}$  state of this complex at 618 nm initiates the intracuster reaction leading finally to the BaF product with ionic binding. In order to elucidate the mechanism of the reaction and to identify possible intermediate states we have first probed the effect of deuteration on the reaction dynamics. We repeated the pump-probe experiment for the complex  $\text{Ba}\cdot\cdot\text{FCD}_3$  at identical laser parameters, *i.e.* with 120 fs laser pulses at a pump wavelength of 618 nm and a probe wavelength of 400 nm. Here the signal analysis yields a decay time of  $430 \pm 20$  fs for the parent ion signal whereas the  $\text{BaF}^+$  ion signal is formed by the superposition of the ionized stable BaF product and a short-living contribution resulting from dissociative ionization of the parent complex.

According to the experimental results obtained and the corresponding *ab initio* calculations the following mechanism for the complete intracuster reaction in  $\text{Ba}\cdot\cdot\text{FCH}_3$  is suggested: After excitation of the parent complex by the femtosecond pulse at 618 nm internal conversion from the  $\tilde{A}$  state to the lower electronic  $\tilde{A}'$  state occurs from which a fast process ( $\tau_R \approx 50$  fs) leads either to the stable BaF product of the charge transfer reaction or to the  $\text{Ba} + \text{CH}_3\text{F}$  fragments in a competing channel. The vibrational energy in the  $\tilde{A}'$  state after internal conversion is sufficient to overcome the barrier for BaF production. Because the time constant of 270 fs for internal conversion is much larger than the decay time  $\tau_R$  of the vibrationally excited  $\tilde{A}'$  state, the duration of the complete intracuster reaction is only slightly larger than the former time constant. Thus, the results of our theoretical and experi-

mental studies presented here have led to a deeper understanding of the basic processes in the intracuster reaction of  $\text{Ba}\cdot\cdot\text{FCH}_3$ .

## Acknowledgements

The authors wish to thank Prof. I. V. Hertel for his continuous support and Prof. A. Gonzalez-Ureña (Universidad Complutense de Madrid) for various fruitful discussions of this work. Financial support by the Deutsche Forschungsgemeinschaft through Sonderforschungsbereich 450 is gratefully acknowledged. The *ab initio* calculations were carried out on the CRAY J932 of the Konrad-Zuse-Zentrum für Informationstechnik Berlin.

## References

- 1 D. R. Herschbach, *Adv. Chem. Phys.*, 1966, **10**, 319.
- 2 K. T. Gillen, C. Riley and R. B. Bernstein, *J. Chem. Phys.*, 1969, **50**, 4019.
- 3 A. H. Zewail, *J. Phys. Chem.*, 1996, **100**, 12701.
- 4 K. Lin, J. C. Polanyi and S. Yang, *J. Chem. Phys.*, 1993, **98**, 5431.
- 5 B. Soep, S. Abbes, A. Keller and J. P. Visticot, *J. Chem. Phys.*, 1992, **96**, 440.
- 6 S. Skowronek, R. Pereira and A. Gonzalez-Ureña, *J. Phys. Chem. A*, 1997, **101**, 7468.
- 7 S. Skowronek, R. Pereira and A. Gonzalez-Ureña, *J. Chem. Phys.*, 1997, **107**, 1668.
- 8 V. Stert, P. Farmanara, W. Radloff, F. Noack, S. Skowronek, J. Jimenez and A. Gonzalez-Ureña, *Phys. Rev. A*, 1999, **59**, R1727.
- 9 P. Farmanara, V. Stert, W. Radloff, S. Skowronek and A. Gonzalez-Ureña, *Chem. Phys. Lett.*, 1999, **304**, 127.
- 10 V. Stert, P. Farmanara, H.-H. Ritze, W. Radloff, K. Gasmi and A. Gonzalez-Ureña, *Chem. Phys. Lett.*, 2001, **337**, 299.
- 11 P. Piecuch, *J. Mol. Struct.*, 1997, **436–437**, 503.
- 12 G. P. Smith, J. C. Whitehead and R. N. Zare, *J. Chem. Phys.*, 1977, **67**, 4912.
- 13 P. J. Knowles and H.-J. Werner, *Theor. Chim. Acta*, 1992, **84**, 95.
- 14 P. J. Hay and W. R. Wadt, *J. Chem. Phys.*, 1985, **82**, 299.
- 15 M. Badoui and J. P. Champion, *J. Mol. Spectrosc.*, 1985, **109**, 402.
- 16 M. A. Dakhil, W. E. Blass, G. W. Halsley and S. J. Daunt, *J. Mol. Spectrosc.*, 1987, **125**, 309.
- 17 J. N. Harvey, D. Schröder, W. Koch, D. Danovich, S. Shaik and H. Schwarz, *Chem. Phys. Lett.*, 1997, **278**, 391.
- 18 Th. Freudenberg, W. Radloff, H.-H. Ritze, V. Stert, K. Weyers, F. Noack and I. V. Hertel, *Z. Phys. D*, 1996, **36**, 349.
- 19 P. Ludowise, M. Blackwell and Y. Chen, *Chem. Phys. Lett.*, 1997, **273**, 211.
- 20 V. Stert, H.-H. Ritze, W. Radloff, K. Gasmi and A. Gonzalez-Ureña, *Chem. Phys. Lett.*, in press.
- 21 CRC Handbook of Chemistry and Physics, ed. D. R. Lide, CRC Press, Boca Raton, FL, 77th edn., 1996.